Response to review with minor comments

Castricum, Netherlands
bas.altena@geo.uio.no

January 8, 2019

Dear editor and reviewers,

Thank you very much for your effort to assess our manuscript. Our apologies for the tedious work you as editor and reviewers had to do, concerning the spelling errors. We have adjusted the minor comments as given by you, and other small errors and spelling has been adjusted, please see the marked-up manuscript.

However not all comments are implemented, specifically one issue, in the following we will give our reasons why we did not. Reviewer #4 points out to an issue which is common for inter-seasonal velocity extraction with optical imagery; shadows in winter cause the pattern matching to fix on the shadows, as an example see figure 1. We have been thinking about how to quantify this issue, but the study in its current form, makes it difficult to implement. There are several reasons why we have not included this aspect in this manuscript:

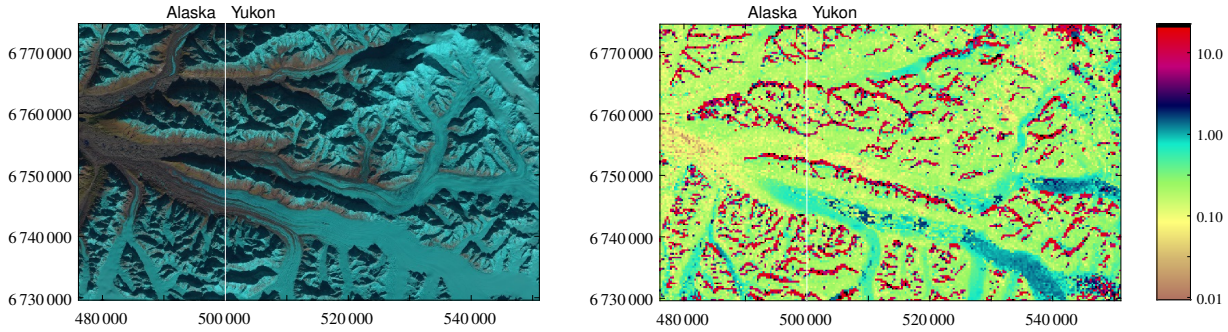

(a) Landsat 8 acquisition on the 8th of August 2016 (b) GoLIVE displacement in March 2014 [m/day].

figure 1: An example of surface displacement of glacier ice (soft colours) and shadow displacements (red) over Walsh Glacier.

The major issue we see is the sparse connection of velocity products. The network in the appendix already shows this issue, where large gaps exist throughout the season. Here one can see that in general the winter velocities are better constrained, while the summer has less coverage. This might result in ill-conditioned estimation of velocity over the summer season. It is a limitation of the GoLIVE product, which has only velocity products ranging up to 96 days. It is not only shadow tracking in winter, which can be a problem. Snow cover and melt-out (which occur in autumn and spring) are therefore the most sensitive time periods for similarity loss. Thus the presented results in this study are on the edge of signal-to-noise, as the redundancy-number is generally low.

Secondly, in the current form the misfit or singularity of the least squares adjustment is not saved. This would be a good indicator for precision, however this would mean the calculation would have to be re-run. In addition it will be questionable if disentangling these factors (correlation, coverage, coherence) is possible. We are working on a follow-up study that does included multiple sensors (Sentinel-1&2) to get longer time-spans and multi-modal velocities. In this way, thorough decomposition and analysis is possible, but this would require re-framing the whole manuscript, and switching the objective of the study. Shifting emphasis from discovery to analysis-ready-data.

Thirdly, the shadow error is dependent on the product used. Normalize cross-correlation is most sensitive to large intensity variation [Debella-Gilo and Kääb, 2011], which the GoLIVE workflow is based upon [Fahnestock et al., 2016]. To reduce this effect the GoLIVE correlator uses imagery which have gone through a high-pass filter [Scambos et al., 1992]. Setting the wavelength of the filter is a subtle trade-off, as at the same time shading and shadowing of smaller surface topography is a feature to correlate (especially in winter). In modern day satellite instruments information is present in the imagery over shadow casted terrain, hence in principle frequency based orientation correlation [Heid and Kääb, 2012] might perform better for this specific issue. To wrap-up, to us this issue more dependents on the input and less on the presented methodology.

The verification as given through the rapidEye pair over Klutlan Glacier could be a solution to assess the influence of shadowing. A different region should be choosen in the upper part of a glacier. But this would mean multi-spectral matching, different processing steps and thus additional information about such steps need to be included into the text. It would deviate from the subject of the paper, but practically it is possible.

The given signal of the shadows in the GoLIVE products might be filtered out through locatization through ray-casting of the sun with the help of a digital elevation model. However, again this is not the scope of the study and as is, the product looks at displacements through surface appearance. Thus the created framework will follow features of the glacier surface and shadow cast, as both comply with the presented framework and do not violate the geometric property. Neighborhood operators (like the common median filter [Paul et al., 2015]) also fail to grasp this effect, and to our knowledge this is still an open issue. Hence, any previous published work will have this signal within, not only displacement fields, but also elevation models derived from optical sensors [Berthier et al., 2005].

To be clear, it is by no means our intention to downplay the concern of the reviewer, as the issue raised by the reviewer is of much interest. But solving or nailing down this issue will result in considerable work, while we think the resulting analysis in the context of this work will not be strong, they might give a hint, but not much insight. If needed, we will do this, but it would mean more time to do so. On the other hand, we hope with the given arguments above you understand the decision not to do so. The claims in our manuscript are intentionally not bold and we hope it shows this direction is work-in-progress, and much can be improved.

Sincerely,

Bas Altena
also on behalf of Ted Scambos, Mark
Fahnestock & Andreas Kääb

Reviewer #4

In the following some specific responses are given to comments given by the reviewers. Missing remarks have been adjusted as suggested, as can also be seen in the new manuscript.

P1, L16: The Gardner et al. (2013) paper is a bit outdated now, as it only considers data up to 2009. A paper such as Harig and Simons (2016) is better as it brings the s.l. contribution record up to 2014.
Thank you, the study was unknown to me.

P4, L6-L8: it would be useful to provide a reference, and perhaps some specific numbers, to back up your statements here. This paper could help: Fleming et al. 2000
Again, thanks for pointing this out, the study is now included.

Fig. 3: I don't understand why the two d1,2 displacements (purple and blue arrows) are different from each other. Please explain.
A more descriptive piece is added.

P8, L7: the lines are described as being blue, purple and yellow, but they look to be blue, purple and orange to me
You are right, the color is "gold", maybe yellow is most suited than.

P9, L5: you mention undersampling as a result of cloud cover, but presumably undersampling could also occur due to snow cover (particularly from new snowfall between image acquisitions)? This follows on from my major comment above.
True, this mention is now included in the text, again this does not the affect the performance of the methodology, as argumented above.

Fig. 5: unclear what needs to extent means in the figure caption. Perhaps this is meant to be written as "needs to extend"?
Changed to enlarged, which might be better to describe the scaling.

P11, L19: it would be useful to provide the distance of the velocity bulge retreat to help the reader understand how significant it is
We have included a flowline time series of the outlet of Hubbard Glacier. It shows our choosen timestep is at the upper limit of resolution, the difference between signal and noise becomes very difficult. More or different data will clearly improve confidence in the product.

Fig. 12a: can you make a comment in the paper as to whether the horizontal stripes in the velocity pattern are real? E.g., are these due to seasonal variability in motion during the surge? Or lack of good velocity matches during the winter?
See former comment.

P20, L18: missing figure number (??). Also reword this sentence, as I have a hard time trying to figure out its meaning: "In the example of Figure ?? the graph is annotated with dates, in order to better understand the other graphs corresponding to other path and rows which are given afterwards."
Sorry, this piece of text was not updated yet, and described the former graphs. It is now updated.

References

E. Berthier, H. Vadon, D. Baratoux, Y. Arnaud, C. Vincent, K.L. Feigl, F. Remy, and B. Legresy. Surface motion of mountain glaciers derived from satellite optical imagery. *Remote Sensing of Environment*, 95(1):14–28, 2005.

M. Debella-Gilo and A. Kääb. Sub-pixel precision image matching for measuring surface displacements on mass movements using normalized cross-correlation. *Remote Sensing of Environment*, 115(1):130–142, 2011.

M. Fahnestock, T. Scambos, T. Moon, A. Gardner, T. Haran, and M. Klinger. Rapid large-area mapping of ice flow using Landsat 8. *Remote Sensing of Environment*, 185:84–94, 2016. doi: 10.1016/j.rse.2015.11.023.

T. Heid and A. Kääb. Evaluation of existing image matching methods for deriving glacier surface displacements globally from optical satellite imagery. *Remote Sensing of Environment*, 118:339–355, 2012.

Frank Paul, Tobias Bolch, Andreas Kääb, Thomas Nagler, Christopher Nuth, Killian Scharrer, Andrew Shepherd, Tazio Strozzi, Francesca Ticconi, Rakesh Bhambri, et al. The glaciers climate change initiative: Methods for creating glacier area, elevation change and velocity products. *Remote Sensing of Environment*, 162:408–426, 2015.

T.A. Scambos, M.J. Dutkiewicz, J.C. Wilson, and R.A. Bindschadler. Application of image cross-correlation to the measurement of glacier velocity using satellite image data. *Remote sensing of environment*, 42(3):177–186, 1992.

Extracting recent short-term glacier velocity evolution over Southern Alaska and the Yukon from a large collection of Landsat data

Bas Altena[1], Ted Scambos[2,3], Mark Fahnestock[4], and Andreas Kääb[1]

[1]Department of Geosciences, University of Oslo, Blindern, 0316 Oslo, Norway
[2]National Snow and Ice Data Center (NSIDC), University of Colorado, Boulder, CO 80303, USA
[3]Earth Science and Observation Center (ESOC), University of Colorado, Boulder, CO 80309, USA
[4]Geophysical Institute, University of Alaska Fairbanks, Fairbanks, AK 99775, USA

Correspondence to: Bas Altena (bas.altena@geo.uio.no)

Abstract. The measurement of glacier velocity fields using repeat satellite imagery has become a standard method of cryospheric research. However, the reliable discovery of important glacier velocity variations on a large scale is still problematic, because time-series span different time intervals and are partly populated with erroneous velocity estimates. In this study we build upon existing glacier velocity products from the GoLIVE data set (https://nsidc.org/data/golive) ~~, we~~ and compile a multi-temporal stack of velocity data over the Saint Elias Mountain range and vicinity. Each layer has a time separation of 32 days, making it possible to observe details such as within-season velocity change over an area of roughly 150 000 km^2. Our methodology is robust as it is based upon a fuzzy voting scheme applied in a discrete parameter space, ~~in this way it~~ and thus is able to filter multiple outliers. The multi-temporal data stack is then smoothed to facilitate interpretation. This results in a spatio-temporal dataset where one can identify short-term glacier dynamics on a regional scale. The goal is not to improve accuracy or precision, but ~~being able to extract~~ to enhance extraction of the timing and location of ice flow events such as glacier surges. Our implementation is fully automatic and the approach is independent of geographical area or satellite system used. We demonstrate this automatic method on a large glacier area in Alaska/Canada. Within the Saint Elias and Kluane mountain ranges, several surges and their propagation characteristics are identified and tracked through time, as well as more complicated dynamics in the Wrangell ~~'s~~ mountains.

1 Introduction

Alaskan glaciers have a high mass turn-over rate (Arendt, 2011) and ~~they~~ contribute considerably to sea level rise ~~(Gardner et al., 2013; Arer~~ (Arendt et al., 2013; Harig and Simons, 2016). Monitoring changes ~~of~~ in ice flow is thus of importance, especially since the velocity of these glaciers ~~seem to fluctuate~~ fluctuates considerably. Many of the glaciers have been identified as surge-type ~~, from~~ based on direct observations or from their looped moraines (Post, 1969; Herreid and Truffer, 2016). Furthermore, ~~topographic~~

~~glacier~~ glacier elevation change in this region is heterogeneous (Muskett et al., 2003; Berthier et al., 2010; Melkonian et al., 2014), ~~which is~~ providing another indication of complicated responses. Gaining a better understanding of ~~the drivers that cause~~ causes of glacier mass re-distribution is ~~therefore of great importance~~necessary in order to separate surging and seasonal variation from longer term trends.

Glacier velocity monitoring through satellite remote sensing has proven to be a useful tool to observe velocity change on a basin scale. Several studies have focused on dynamics of individual glaciers in Alaska ~~,~~at an annual or seasonal resolution (Fatland and Lingle, 2002; Burgess et al., 2012; Turrin et al., 2013; Abe and Furuya, 2015; Abe et al., 2016). Such studies can give a better understanding of the specific characteristics of a glacier, and which circumstances are of importance for this behaviour and response. Region-wide annual or "snapshot" velocities also have been estimated over the Saint Elias Mountain range in previous studies ~~(Burgess et al., 2013; Waechter et al., 2015). Their~~ (Burgess et al., 2013; Waechter et al., 2015; Van Wychen et al., 2018). The results give a first-order estimate of the kinematics at hand. With frequent satellite data coverage, one study found it is possible to detect the time of glacier speed-ups to within a week (Altena and Kääb, 2017b), although ~~the~~ this study did not include an automated approach. In the most recent work, regional analyses have been conducted ~~with~~ over sub-seasonal (Moon et al., 2014; Armstrong et al., 2017) and multi-decadal (Heid and Kääb, 2012a; Dehecq et al., 2015) periods. With such data one is able to observe the behaviour of groups of glaciers that experience similar climatic settings. Consequently, surges and other glacier-dynamical events can be put into a wider spatio-temporal perspective.~~In this contribution we want to develop the methodological possibilities further and try to extract glacier velocities at a monthly resolution over a large region. The presented method retains spatial detail present in the data and does not simplify the flow structure to flowlines. Consequently, we want to improve knowledge about the influence and timing of tributary and neighbouring ice flow variations.~~

Since the launch of Landsat 8 in 2013 a wealth of high-quality medium-resolution imagery is being acquired over the cryosphere on a global scale. Onboard data storage and rapid ground-system processing have made it possible to almost continuously acquire imagery. The archived data has enormous potential to advance our knowledge ~~in~~ of glacier flow. Extraction of glacier velocity is one of the stated mission objectives of Landsat 8 (Roy et al., 2014). ~~However, the~~ The high data rate far exceeds the possibilities for manual interpretation. Fortunately, automatically generated velocity products are now available (Scambos et al., 2016; Rosenau et al., 2016), though at this point sophisticated quality control and post processing methods are still being developed.

Up to now, most studies of glacial velocity have had an emphasis on either spatial or temporal detail. When temporal detail is present, studies focus on a single or a handful of glaciers (Scherler et al., 2008; Quincey et al., 2011; Paul et al., 2017). On the other hand, when regional assessments are the focus, the temporal resolution ~~ranges~~ covers a single period from a single time stamp up to annual ~~resolution~~coverage (Copland et al., 2009; Dehecq et al., 2015; Rosenau et al., 2015). ~~Furthermore, most~~ Most studies rely on filtering in the post-processing of vector data by using the correlation value (Scambos et al., 1992; Kääb and Vollmer, 2000) or through median filtering within a zonal neighborhood (Skvarca, 1994; Paul et al., 2015). Some

sophisticated post-processing procedures are available (Maksymiuk et al., 2016), but rely on ~~the coupling with models based upon the Navier-Stokes equations. Also~~ coupling with flow models or geometric properties can be taken into account during the matching to improve robustness and reduce post-processing efforts, such as reverse-correlation (Scambos et al., 1992; Jeong et al., 2017) or triangle closure (Altena and Kääb, 2017a).

~~Thus~~ While glacier velocity data is increasingly available, ~~but~~ in general post-processing is not at a sufficient level to directly exploit the full information content within these products. In this study we ~~aim at~~ describe the construction of a post-processing chain that is capable of extracting temporal information from stacks of noisy velocity data. Our emphasis is on discovering temporal patterns over a mountain-range scale. Analysis of the ~~individual details of the~~ details of glacier-dynamical patterns identified by ~~the~~ this processing will be considered in later work. For a single glacier, ~~a~~ it is certainly possible to employ manual selection of low-noise, good-coverage velocity data sets~~is possible~~. However, such a strategy will not be efficient when multiple glaciers or mountain ranges are of interest. In this contribution we want to develop the methodological possibilities further and try to construct glacier velocities at a monthly resolution over large areas. Therefore, our implementation focuses on automatic post-processing, without the help of expert knowledge or human interaction. Our method retains spatial detail present in the data and does not simplify the flow structure to flowlines. This methodology can generate products that improve our knowledge about the influence and timing of tributary and neighbouring ice flow variations.

~~In this study, we discuss~~ We start by discussing the data used and provide background on the area under study. We then introduce the spatio-temporal structure of the data, followed by an explaination of our process for vector "voting" and vector field smoothing. The ~~next~~ final section highlights our results and our validation and assessment of the performance of ~~our~~ the method.

2 Data and study region

2.1 GoLIVE velocity fields

The Global Land Ice Velocity Extraction from Landsat 8 (GoLIVE) velocity fields used in this study are based upon repeat optical remote sensing imagery and are distributed through the National Snow and Ice Data Center ~~(NSIDC) (Scambos et al., 2016) .~~ (NSIDC; https://nsidc.org/data/golive) (Scambos et al., 2016). These velocity fields are derived from finding displacements between pairs of Landsat 8 ~~imagery~~images, using the panchromatic band with 15 meter resolution. A high-pass filter of one kilometer spatial scale is applied before processing. Normalized cross-correlation is applied between the image pairs on a sampling grid with 300 meters spacing (Fahnestock et al., 2016; Scambos et al., 1992) and a template size of 20 pixels (or 300 m). The resulting products are grids with lateral displacements, the absolute correlation value, signal-to-noise ratio and ratio between the two best matches. At the time of writing, displacement products can cover a time interval from 16 days up to

96 days. For a detailed description of the processing chain see Fahnestock et al. (2016).

The Landsat 8 satellite has a same-orbit revisit time of 16 days and a swath width of 185 km. Only scenes which are at least 50% cloud-free are used (as determined by the provided estimate in the metadata for the scenes). Consequently, not every theoretical pair combination is ~~matched, and also pairs across tracks are neglected~~ processed, and no pairs of overlapping images different orbits (paths) are used (cf. (Altena and Kääb, 2017a)) to avoid more complicated viewing geometry adjustments. Georeference errors are compensated by the estimation of a polynomial bias surface through areas outside glaciers (i.e., assumed stable). The glacier mask used for that purpose is from the Randolph Glacier Inventory (RGI) (Pfeffer et al., 2014). The resulting grids come in Universal Transverse Mercator (UTM) projection and if orthorectification errors are minimal, displacements for precise georeferencing require only horizontal movement of a few meters (generally <10 m). In total we use twelve Landsat path/row tiles to cover our study area (Figure 1).

2.2 Study region

The region of interest covers the Saint Elias, Wrangell and Kluane Mountain ranges, as well as some parts of the Chugach range. Many surge-type glaciers are located in the Saint Elias Mountains (Post, 1969; Meier and Post, 1969). These ranges host roughly 42 000 km^2 ~~glacier area, whereby~~ of glacier area with roughly 22% of the glacier area ~~is~~ connected to marine terminating fronts draining into the Gulf of Alaska (Molnia, 2008). The glaciers in this area are diverse, as a wide range of thermal conditions (cold and warm ice) and morphological glacier types (valley, icefields, marine terminating) occur in these mountain ranges (Clarke and Holdsworth, 2002). This ~~might partly be~~ diversity is in part due to the large precipitation gradient over the mountain range. The highest amount of precipitation falls in summer or autumn. The study area covers mountain ranges ~~that have two different clusters of climate~~with two distinct climates. Along the coast one finds a maritime climate with a small annual temperature range. These mountains function as a barrier, and the mountain ranges behind, in the interior, have ~~therefore~~ a more continental climate (Bieniek et al., 2012).

3 Methodology

GoLIVE and other similar velocity products are ~~composed products~~ developed from at least two satellite acquisitions. When ~~imagery~~ images from multiple time instances are used, combinations of displacements, with different (overlapping) time intervals can be constructed. In order to be of use for ~~time-serie analysis, such~~ time-series analysis, detailed velocity fields with different time spans need to be combined into a dataset with regular timesteps. To reduce the noise, the temporal configuration of ~~these~~ overlapping products can be used to synthesize ~~a~~ am improved multi-temporal velocity field.

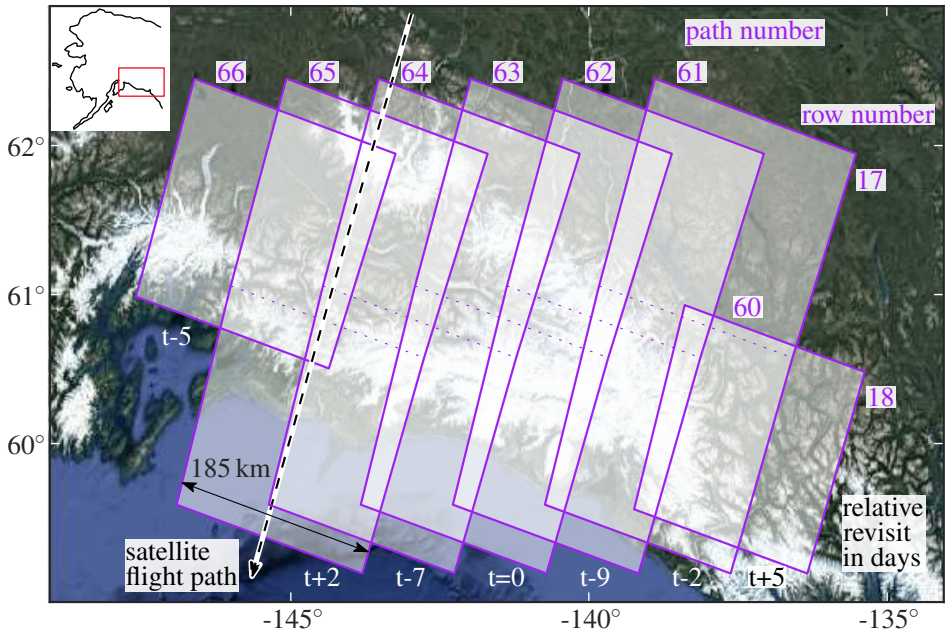

Figure 1. Nominal Landsat 8 footprints used over the ~~studied~~ study region. The purple text ~~colors~~ annotates the different satellite paths of LANDSAT, while the black text indicates the relative overpass time in days in respect to path 63.

3.1 Temporal network configuration

At the ~~high latitude of the Southern Alaska~~latitude of Southern Alaska, scenes from adjacent tracks have an overlap of 60%. Looking at only one track (or ~~satellite~~ Landsat path), the 16-day revisit makes several matching combinations of integer multitudes of 16 days possible. For example, over a ~~64-days~~ 64-day period (Δt), five images are acquired ~~in~~ from one satellite track and their potential pairing combinations can be illustrated as a network (Figure 2). In this network, every acquisition (at time t) is a node, and these nodes are connected through an edge that represents a matched pair leading to a collection of displacements (d) with ~~an~~ associated similarity measures (ρ).

When velocities over different timespans are estimated, this network has in theory a great amount of redundancy. However in practice this is complicated, as combinations of images are not processed when there is too much obstruction by clouds. Furthermore, individual displacements can ~~be~~ have gross errors, as an image match was not established due to surface change or lack of contrast and thus loss of similarity. Consequently, when data from such a network is combined to synthesize one consistent velocity time series the estimation procedure needs to be able to resist multiple outliers or be able to identify whether displacement estimates could be extracted at a reliable level at all.

The network shown in ~~figure~~Figure 2 can be seen as a graph; nodes correspond to timestamps and edges to matched image pairs. Such a graph can be transformed into an adjacency matrix ($\mathbf{A}_G$, see Figure 2). In this matrix the columns and rows

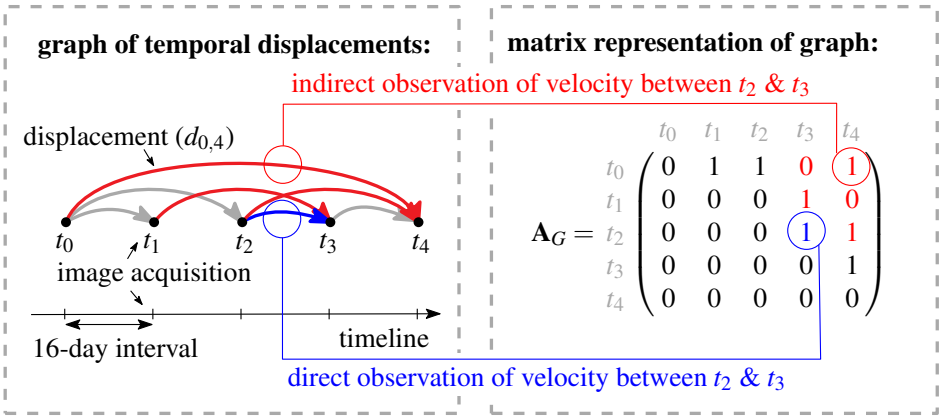

Figure 2. Graphical and matrix representation of a network. Here acquisition pairs within a network are illustrated and written down in an adjacency matrix ($\mathbf{A}_G$). The dark gray squares indicate acquisitions within a period to be estimated. The connecting colors symbolize an open (red) or closed (blue) selection of displacements to be used for the velocity estimation over this period ($\mathbf{v}$).

represent different timestamps. The edges can be directed, ~~meaning it can assign~~ indicating which acquisition is the master (reference) or the slave (search) image during the matching procedure. For the GoLIVE data, the oldest acquisition is always the reference image, hence within the matrix only the upper triangular part has filled entities. The spacing of the timesteps is 16 days and the ~~amount~~ number of days is set into the corresponding entries when a time step is covered by an edge. Individual days are specified ~~instead of a binary entity, to be able to merge~~ so that adjacency matrices from different tracks which have different ~~acquiring dates~~ acquisition dates can be merged. If partial overlap of an edge occurs, then the time steps are proportionally distributed. For example, for a small network of three nodes, velocity (v) can be estimated through ~~least-square~~ least-squares adjustment of the displacements (d) through the following systems of equations (Altena and Kääb, 2017a),

$$\mathbf{y} = \mathbf{A}\mathbf{v}, \text{ where } \quad \mathbf{y} = \begin{bmatrix} d_{12} \\ d_{23} \\ d_{13} \end{bmatrix}, \quad \mathbf{A} = \begin{bmatrix} \Delta t_{12} & 0 \\ 0 & \Delta t_{23} \\ \Delta t_{12} & \Delta t_{23} \end{bmatrix}, \quad \mathbf{v} = \begin{bmatrix} v_{12} \\ v_{23} \end{bmatrix}, \tag{1}$$

Here the subscript denotes the timespan given by the starting and ending timestamps of the interval. This relational structure of displacements is similar to a leveling network. When the adjacency matrix is converted to an incidence matrix, then this matrix is the design matrix ($\mathbf{A}$) (Strang and Borre, 1997). This makes the generation of such network adjustments easily implemented.

This formulation of the temporal network makes it possible to estimate the unknown parameters, i.e. the temporal components of the velocity time series, through different formulations. This is illustrated in Figure 2, where a ~~selection of a~~ velocity (between t_2 & t_3) is estimated. Displacements that fall between the two images can be used for the estimation (here blue), which we here call a "closed" network. But as can be seen in the figure as red connections, other displacements from outside

the time span are over-arching and stretching further than the initial time interval. Such measurements can be of interest as they can fill in gaps or add redundancy, but the glacier ~~dynamics~~ flow record obtained will be ~~smeared~~ aliased compared to the real ~~ones~~motion. Consequently, we call such a network configuration an "open" network (here red).

3.2 Voting

The velocity dataset we use (like any) contains a large ~~amount~~ number of incorrect or noisy displacements. Typically, the distribution of displacements has a normal distribution but with long tails. Moreover, a ~~least-square~~ least-squares adjustment is very sensitive to outliers contained in the data to be fitted. Therefore, direct ~~least-square~~ least-squares computation of velocity through the above network is not easily possible and some selection procedure is needed to exclude gross errors. Outlier detection within a network such as in equation 1 can be done through statistical testing (Baarda, 1968; Teunissen, 2000), assuming measurements (d) are normally distributed. However, such procedures are less effective when several gross errors are present within the set of observations. Extracting information from highly contaminated data is therefore an active field of research. For example, robust estimators change the normal distribution to a heavy tailed distribution. Nevertheless, such estimations typically still start with normal least-squares adjustment based on the full initial set of observations, and only in the next step the weights are iteratively adjusted according to the amount of misfit. Hence, such methods are still restricted to robust a-priori knowledge or a data-set with relatively small amounts of contamination by gross errors.

Another common approach to cope with the adjustment of error-rich observations is through sampling strategies such as least-median of squares (Rousseeuw and Leroy, 2005), or random sampling and consensus (RANSAC) (Fischler and Bolles, 1981). A minimum ~~amount~~ number of observations are picked randomly to solve the model. The estimated parameters are then used to assess how the initial model fits in respect to all observations. Then the procedure is repeated with a new set of observations. The sampling procedure is stopped when a solution is within predefined bounds, or executed a defined ~~amount~~ number of times after which the best set is taken. Such methods are very popular as they can handle high contamination of data (up to 50%) and still result in a correct estimate. Put differently, the break-down point is .5 (Rousseeuw and Leroy, 2005). However, we use a different approach as these methods implement polynomial models. Our data set benefits from including conditional equations as well.

The equations that form the model can be seen as individual samples that populate the parameter space. In such a way the individual relations within the equation propagate into points, lines, or surfaces depending on their dimensions and relation given by the equation. Hence, measurements can be transformed into a shape that is situated within the parameter space (which has a finite extent and resolution). The collection of shapes will be scattered ~~through out~~ throughout this parameter space, but such ~~shape~~ shapes converge at a common point which is most likely the correct parameter values. This transformation is the Hough transform and is commonly used in image processing for the detection of lines and circles.

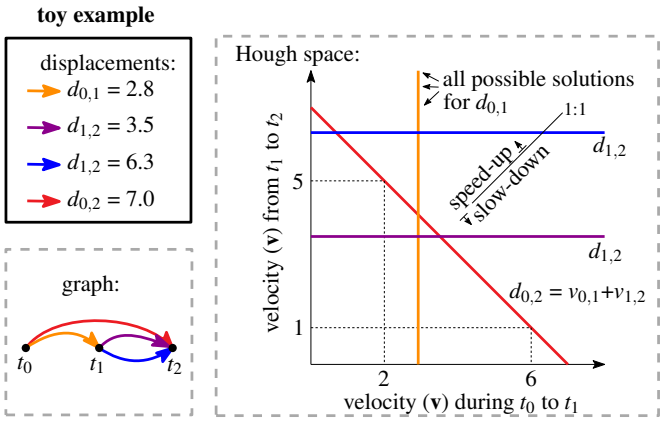

Figure 3. On the left is a graphical representation of Landsat 8 acquisitions at different times (t) illustrated as nodes and matching solutions with displacements (**d**) are shown as edges, within a network. The subscript for the displacement denotes the time interval. The velocities (**v**) are estimated through the collection of all these displacements. On the right the mathematical representation or its parameter (Hough) space for voting of displacements over two time instances is shown, in this case the parameter space of only $\mathbf{v}_{0,1}$ & $\mathbf{v}_{1,2}$ are shown.

However, the Hough transform is discrete while the measurements are noisy, thus the shapes should also be fuzzy. In this study we follow this latter direction and ~~discretize~~ after discretizing the displacement-matching search-space~~after which ,~~ we exploit a voting strategy. ~~But~~ Because the shapes in parameter space are blurred, ~~so~~ a fuzzy Hough transform (Han et al., 1994) is implemented. Our matching search space is simply the linear system of equations of the network described above. To illustrate the system, an example of a network with four displacements (**d**) is shown in Figure 3. These displacements can be placed within a discrete grid that spans a large part of the parameter space (in this example two dimensional). For the short time span displacements, this results in vertical or horizontal lines (blue, purple and ~~yellow~~orange). The lines originate from the ambiguity, which is also in the entries of the design matrix (**A**) as ~~these are~~ 0 entries. For the overarching displacement (in red) the displacement is a combination of both velocities. Only the total displacement is known, thus the line results in a diagonal orientation ($5+2$ can be a solution as well as $1+6$, or a non-integer combination).

In this toy example, the lines concentrate around 3 for both velocities, but with a slight preference to the upperleft~~, which~~ . This location indicates a slight speed-up between these two ~~timespans~~time spans. ~~However, the lines are~~ For this case, the blue line is an outlier; it does not contribute to crossings in this zone, and instead creates single crossings with other correct displacements at other locations within the parameter space. Apart from the blue line, the other crossings are concentrated around a zone, but are not perfectly intersecting ~~, as measurement noise is present~~at a single point. This is due to noise present in every displacement measurement. To simulate this noise, the lines are perturbed with a Gaussian function, as for the toy example shown in ~~figure~~Figure 4a. In this case, every observation will fill the parameter space with a discretized weighting function. This fuzziness in the Hough space makes it possible to find the intersection ~~,~~ while noise is present. ~~Furthermore,~~ ~~the~~ The dimension of the Hough space ~~dependents~~ depends on the formulation of the network. In principle it can have any

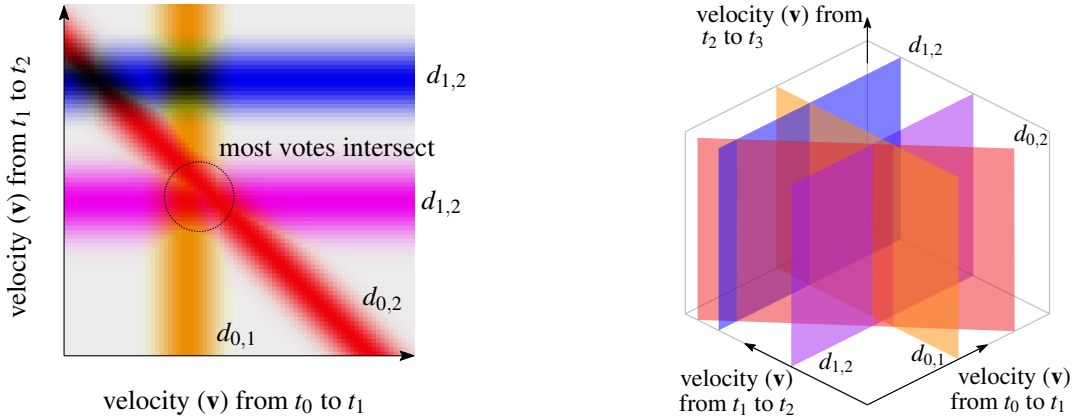

(a) two dimensional fuzzy Hough space

(b) three dimensional Hough space.

Figure 4. Two modifications used in this study, which deviate from the standard Hough-transform as given by the toy example in figure 3. (a) the change from a clear ideal line, towards fuzzy weights. (b) the extension towards a higher dimension, in this case the lines transform to planes, that intersect with each other.

dimension; in one ~~dimensional case~~ dimension this is a simple histogram, but in higher dimensions this will translate into a line which radially decreases in weight. For this study we implement a three-dimensional Hough space, which for our toy example will look like ~~as in figure~~Figure 4b, though due to visualization limitations, the fuzzy borders are not ~~visualized~~included.

The advantage of a Hough search space is the resistance to multiple outliers. It builds support and is not reliant on the whole group of observations. ~~Especially, when~~ When a second or third dimensional space is used, the chances of random (line) crossing ~~decrease significantly in parameter space. Hence,~~ decreases significantly in the parameter space, and such events will stand out when multiple measurements do align. ~~Furthermore, random~~ Random measurement errors can be incorporated through introducing a distribution function. In our implementation this is a Gaussian, but other functions are possible as well. The disadvantage of the fuzzy Hough transform is its limitation ~~to implement~~ in implementing a large and detailed search space, as the dimension and resolution depend on the available computing resources.

The fuzzy Hough transform functions as a selection process to find observations which are to a certain extent in agreement. With this selection of inliers the velocity can finally be estimated through ordinary least-squares estimation. The model is the same as used to construct the network. However, the observations without consensus (i.e. outliers) are not used. The remaining observations can, nevertheless, still be misfits, such as from shadow casting, as no ice flow behavior is prescribed in the design matrix of equation 1.

3.3 Smoothing

Because the voting and least-squares adjustment in our implementation has no neighborhood constraints but is rather strictly per matching grid point, the velocity estimates contain systematic, gross and random errors, though reduced with respect to the initial data set. This least squares adjustment with voted displacements results in a spatio-temporal stack of velocity estimates that have a regular temporal spacing. However, due to undersampling as a result of cloud cover or lack of consensus between the displacement acquisitions, the stack might have holes or ill-constrained estimates. We apply a spatial-temporal smoothing taking both spatial and temporal information into account using the Whitacker approach that tries to minimize the following function (S),

$$S = \sum_i w_i (\hat{x}_i - x_i)^2 + \lambda \sum_i (\Delta^2 x_i)^2. \tag{2}$$

This formulation is the one dimensional case, where for every location (x, where i denotes the index of the grid) an estimate (denoted by $\hat{\cdot}$) is searched for that minimizes S. Here Δ denotes the difference operator, thus $\Delta x_i = x_{i+1} - x_i$. Similarly, Δ^2 is the double difference, describing the curvature of a signal (~~$\Delta^2 x_i = x_{+1} - 2x_i - x_{i-1}$~~ $\Delta^2 x_i = x_{+1} - 2x_i + x_{i-1}$). For the implementation of this method we use the procedure presented by Garcia (2010). This routine has an automatic procedure to estimate the smoothing parameter (λ) and has robust adaptive weighting (w). Its implementation ~~is conducted through~~ uses a Discrete Cosine Transform (DCT), which eases the computational load. ~~Furthermore, a~~ The discrete cosine transform operates both globally and locally, and in multiple dimensions. ~~Lastly, in~~ In order to include all data at once, the vector field is configured as a complex number field.

The smoothing parameter (λ) is operating over both space (2 dimensions) and time (1 dimension), but the smoothing parameter is a single scalar. ~~Hence in~~ In this form it would be dependent on the choice of grid resolutions in time and space. ~~Therefore, in~~ In order to get rid of this dependency and fulfill the isotropy property, the spatial and temporal dimensions are scaled. For this scaling estimation we construct an experimental variogram and look at its distribution (Wackernagel, 2013). Along the spatial axis, the variogram in Figure 5a shows spatial correlation up to about 10 kilometers. This sampling interval is then used to look at the spatio-temporal dependencies, as illustrated in Figure 5b. ~~Around~~ At around a year temporal distance ~~,~~ one can see a clear correlation ~~,~~ which corresponds to the seasonal cycle of glacier velocity. From this variogram a rough scaling was estimated, and the anistropy was set towards a factor of four. In our case the pixel spacing is 300 meters and the time separation is 32 days.

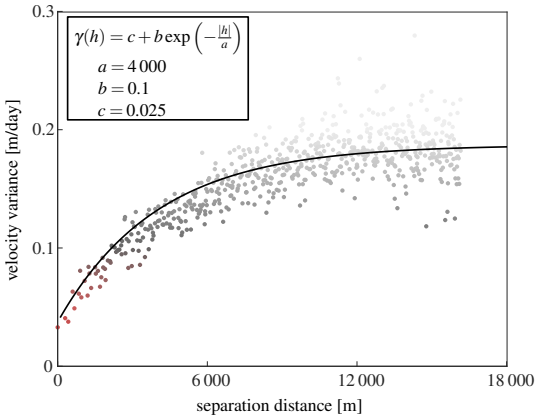

(a) Experimental variogram in the spatial domain

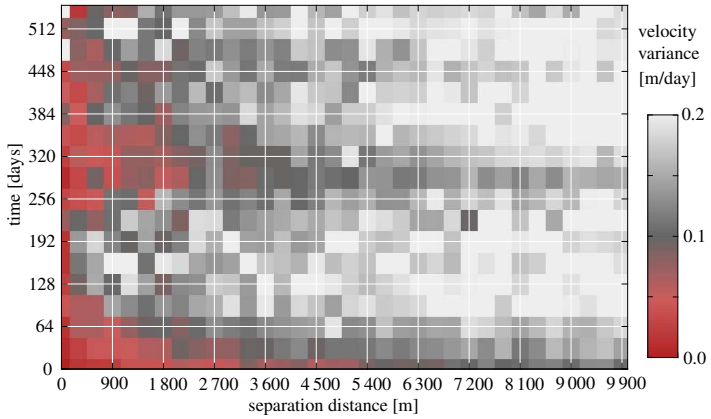

(b) Spatio-temporal experimental variogram

Figure 5. Experimental variograms over a slice of the stack and over a subset of the spatio-temporal stack.The colorbar along the axis of figure 5a, is used for the coloring of figure 5b. The aspect ratio of figure 5b is at the resolution of the produced data-cube (32 days by 300 meters). In order to make this isotropic, the vertical axis needs to ~~extent~~enlarge, so the spread in variance is similar in ~~both directions~~any direction (isotropic).

4 Results

4.1 Method performance

Two different temporal networks (combinations of time intervals) can be formulated in order to calculate a velocity estimate, as is described in section 3.1. The "open" configuration includes a greater number of velocity estimates from image pairs, but this has consequences. It results in a more complete dataset, with coherent velocity fields, but when short-term glacier dynamics occur, temporal resolution of the event may be ~~smeared~~aliased.

Our methodology thrives when several displacement estimates are present, otherwise testing is not possible. This prerequisite is especially apparent when a "closed" configuration is used, then the collection of displacements are reduced. In order to show this dependency a slice is shown in Figure 6~~, in~~ . In this time interval the ~~Western~~ western side has several overlapping displacement estimates in space and time, while this is limited at the ~~Eastern~~ eastern side. The exact distribution of the available data for this time interval is also highlighted in Figure A1, within the appendix. The lack of data can be seen at the western border of both ~~both~~ estimates. On the eastern side the glacier velocity structure is more clearly visible~~. Especially~~ , especially in the "open" configuration .

In Figure 7 more details of the two different configurations are shown. ~~However, by~~ By including more imagery as with an open configuration, the velocity estimates are more complete, as can be seen along the outlets of Guyot Glacier. In the same subsection, ~~not only the completeness increase but also the consitency~~the completeness increases and so does the consistency,

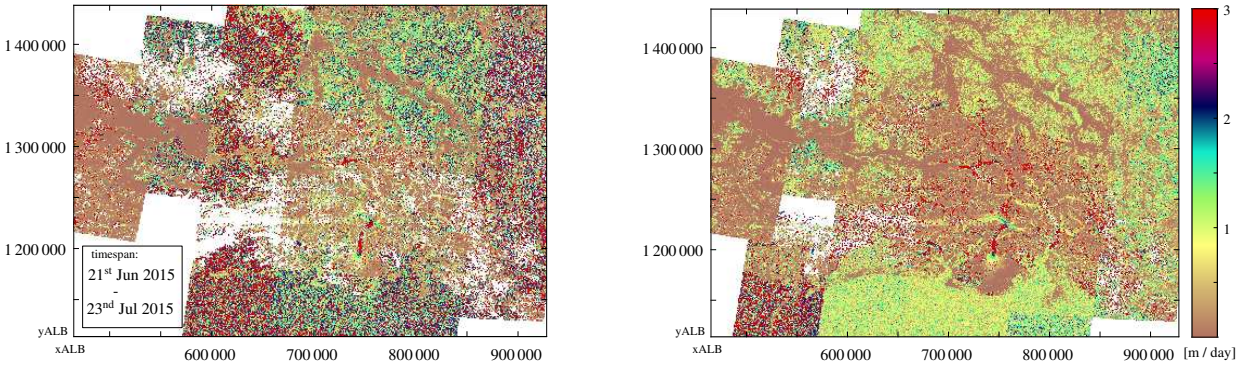

(a) Closed network selection

(b) Open network selection

Figure 6. Least square estimates of velocities with different network configurations, see Figure 3 for a toy example of the terminology. The study region spread over several UTM zones, hence the dataset is in Albers equal-area projection (ALB) with North American Datum 83. White regions correspond to data without an estimate.

which is ~~mostly appearant by~~ most apparent in the coherent low velocities over stable ground. With more displacement vectors in the configuration, smaller-scale details, such as tributaries flowing into the large Kaskawulsh glacier, become more evident.

The spatio-temporal ~~least-square~~ least-squares estimates still have to some extent variation in direction and amplitude as well as outliers. Therefore spatial-temporal smoothing is applied, in order to extract a better overview from the data, as is described in section 3.3. The results of this smoothing for the same time interval as in Figure 6 is shown in Figure 7.

In the smoothing procedure the surroundings of glaciers, which are stable- or slow moving terrain, are included. Consequently, high speed-ups such as on the surge bulge on the Steele glacier are dampened, as in this case it has a confined snout within a valley. They do not disappear, as the signal is strong and persistent over time, but damping does occur. An aspect of concern is the ~~velocity bulge retreat of~~ retreat of the high velocity termini of many outlet glaciers; their fronts with large velocities seem to retreat in the smoothed version, while this is not the case for the original least-squares estimate ~~. This is an effect~~ (see example in Appendix B). This effect is caused by surrounding zero-valued water bodies. Damping also occurs at turns such as at Hubbard glacier, where the mask reduces the ~~mask does reduce the~~ effect of stable terrain, but has no specific glacial properties. The isotropy function included ~~into~~ in the smoother might work for ~~the direct~~ a local neighborhood, but breaks down for fast moving outlets. For this smoother, weights are given in relation to a neighborhood. However for glacier flow, the magnitude might be more similar in the direction of ~~the~~ flow lines, while in the cross-flow direction the flow orientation might be more similar. This relation is not included in the smoother~~and therefor damping occurs. Nonetheless,~~ , causing damping of the gradients. There is a trade-off between the damping effect of the smoothing ~~outweighs~~ and the advantage of having a clear image ~~and overview over the mountain ranges~~over large areas.

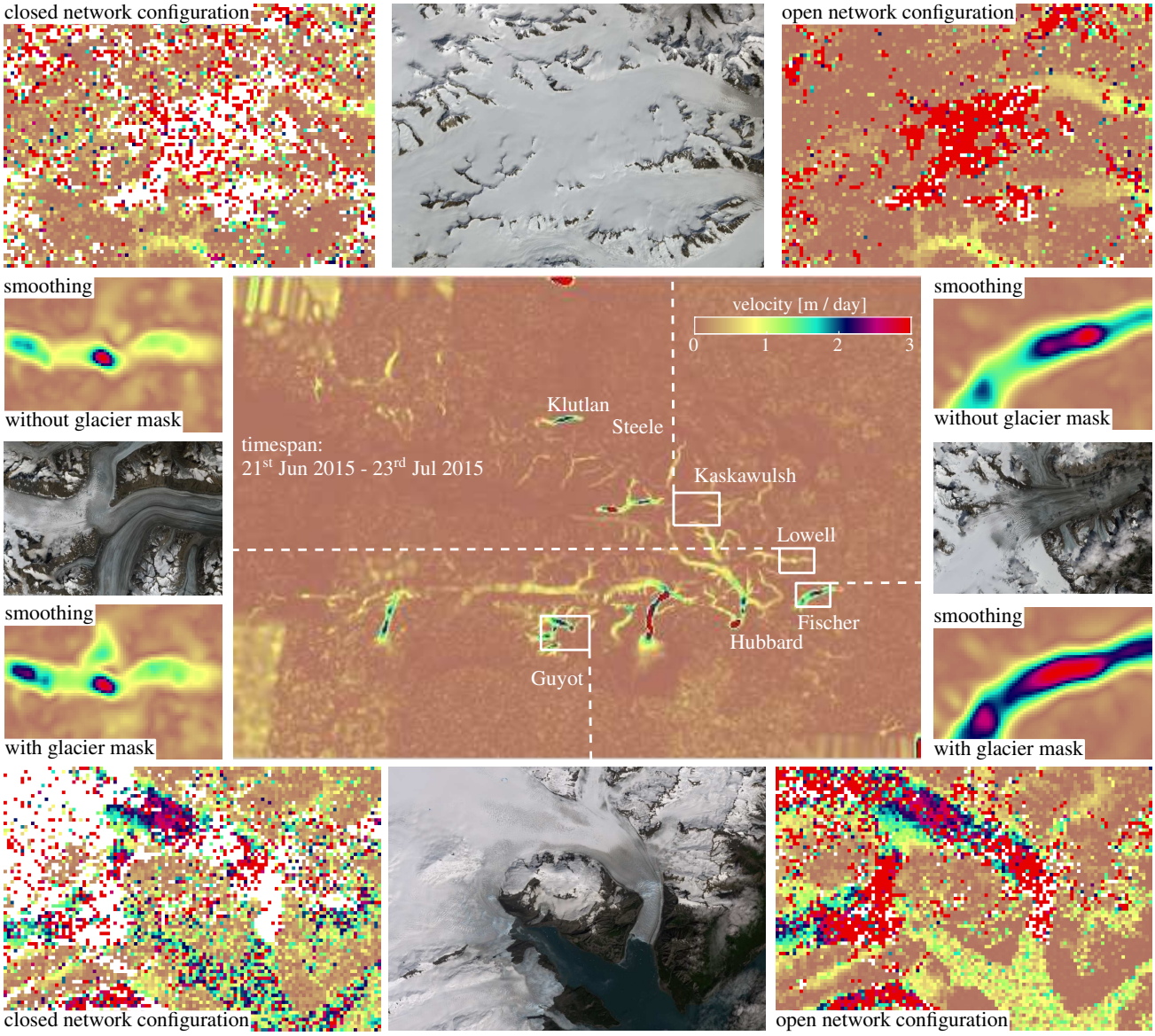

Figure 7. Overview map of different sections for the time interval which is similar to Figure 6 (i.e: 21st of June till 23th of July 2015). The surrounding zoom-ins are from the same time period, but with different configurations (open vs closed) or smoothing settings (glacier mask vs. no-mask).

Because the surrounding terrain, which has no movement, impacts the smoothed glacier velocity estimates, in particular for surge and calving fronts (i.e. for strong spatial velocity gradients), the smoothing can be supported by a glacier mask. In our case, this mask is a rasterization of the Randolph Glacier Inventory (Pfeffer et al., 2014), with an additional dilation operation, to take potential advance or errors in the inventory into account. The difference in result ~~for~~ using this masking procedure is shown in Figure 7, with some highlights. In general, the mask does compensate a little bit for the damping, but because the regions are mostly covered with ice its effect is small.

4.2 Validation of post-processing procedures

The voting used in our procedure is assessed through validation with an independent velocity estimate. Terrestrial measurements are limited in the study area, hence we use satellite imagery from RapidEye satellites over a similar timespan. Data from this constellation has a resolution of 5 meters and through processing in a pyramid fashion, a detailed flow field can be extracted. This velocity field functions as a baseline dataset to compare the GoLIVE and the synthesized data. Here we will look at a section of Klutlan Glacier, which flows from west to east ~~,~~ and is thus aligned with one ~~of the~~ map axis. The velocity of this glacier is, due to its surge, of significant magnitude, and ~~therefor~~ therefore will have a wide spread in the voting space.

The two RapidEye images used over Klutlan Glacier were taken on 7th of September, and on 7th of October 2016. To retrieve the most complete displacement field of the glacier, we used a coarse-to-fine image matching scheme. The search window decreased stepwise (Kolaas, 2016) and the matching itself was done through Orientation Correlation (Heid and Kääb, 2012a). At every step a local post-processing step (Westerweel and Scarano, 2005) was implemented, to filter outliers. The resulting displacement field over one axis (that is x, the general direction of flow) for this period is illustrated in the upperleft inset of Figure 8.

For the voting of the Landsat 8-based GoLIVE data, an overlapping time period was chosen, from the 11th of September up to the 13th of October 2016, nearly but not exactly overlapping with the RapidEye pair. An "open" configuration was used~~for the voting~~, meaning all GoLIVE displacement fields covering this time period were used, resulting in a total of 36 velocity fields involved in the voting. The voted estimates and scores are illustrated ~~at~~ in the lower panels of Figure 8. Voting scores are high over the stable terrain, but low over the glacier trunk. To some extent this can be attributed to the surge event. The median over the stack and the median of absolute differences (MAD) are shown on two panels ~~at~~ on the right side of ~~figure~~Figure 8. These two measures are frequently used to ~~produce and~~ analyze multi-temporal datasets (Dehecq et al., 2015).

When looking at this time period for the GoLIVE data, a clear displacement field is shown, as both images (11th Sept., 13th Oct.) from Landsat 8 were cloud free. The pattern is in close agreement with the RapidEye version. When looking at the voted estimate a similar pattern is observable but more corrupted. In some ~~respect~~ respects the median estimate ~~grasps~~ captures the direction of flow, but over estimates the velocity, probably due to the surge that occurs. The spread might confirm this, as shown

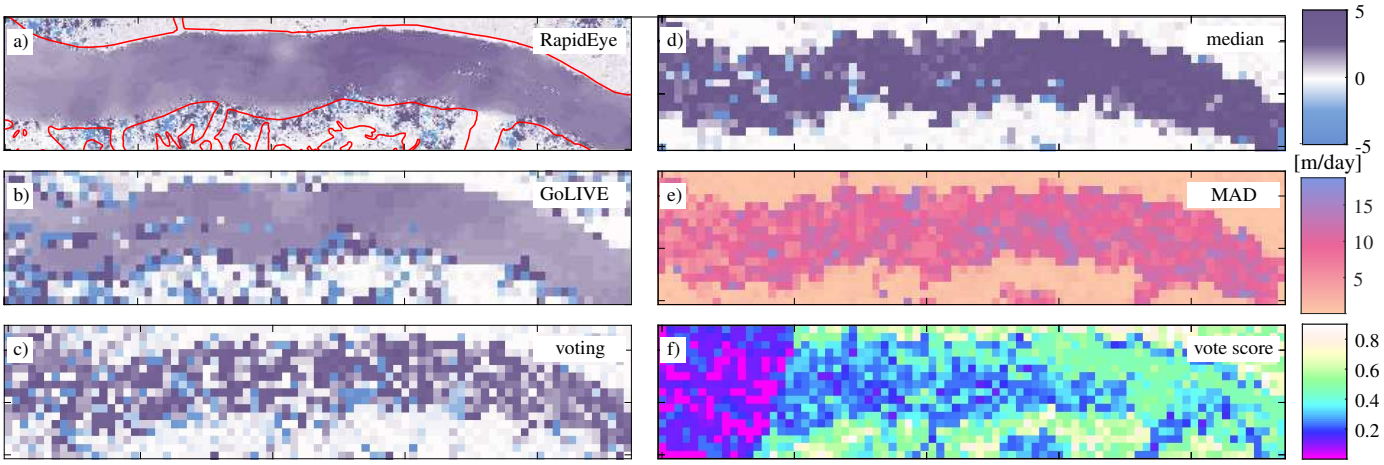

Figure 8. Monthly displacement in x-direction over the Klutlan Glacier (for location see Figure 7) using several data sources and velocity assessment schemes. The top panel shows velocities derived from two RapidEye images (a). Glacier borders are outlined in red. The second figure shows displacement estimates from a GoLIVE dataset ((b),input), and the resulting voted estimate (c) of a combination of 36 GoLIVE datasets (output). Its corresponding voting score (f) of these estimates is shown in the ~~fourth~~ lower right figure. The ~~last~~ two upper right most figures show the median of absolute deviation (MAD) (e) and the median (d) over the full dataset. These last two results would typically be used for data exploration.

by the MAD, as this is considerable and will not help to justify which displacement is correct. Furthermore, the voted estimate is an estimate over a short interval, while the median estimate is calculated over the full stack.

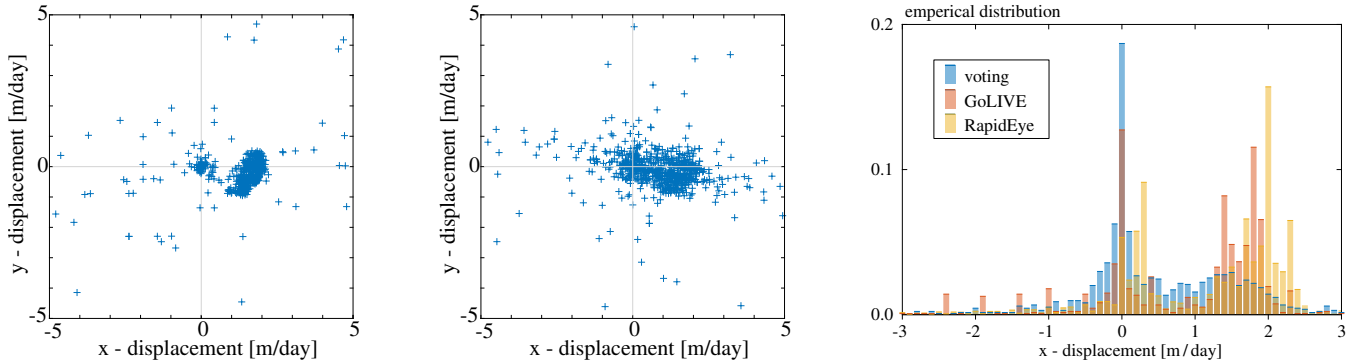

(a) velocity distribution GoLIVE (b) velocity distribution voting (c) distribution x-displacement

Figure 9. Figure 9a & 9b show the distribution of velocities for a section of Klutlan glacier, their map view are shown in Figure 8. In figure 9c the same x-component data as in Figure 8 is shown, but now the distributions are shown.

To better assess these results, the distribution of both ~~two-dimenstional~~ two-dimensional displacement fields are illustrated in Figure 9a and 9b. Two groups of displacement regimes are clearly visible, a cluster showing little movement, ~~or a flock~~ and a group of displacements with a dominant movement eastwards. The voted distribution has more spread, and outliers are present, but in general the mapping has the correct direction and magnitude. When the x-component of these displacements ~~are~~ is compared against the RapidEye displacements~~. The~~ , the median of this difference is 0.45 ~~mtr~~m/day for the voting and 0.27 ~~mtr~~m/day for the good GoLIVE pair. A similar trend can be seen in Figure 9c, which again shows the distributions are similar. ~~Hence, the illustrated validation~~ The illustrated validations do show the voting scheme is able to ~~grasp~~ capture the general trend of the short term glacier flow through a large stack of corrupted velocity fields. While the voted estimate is worse than the clean GoLIVE estimate, we stress that the chosen GoLIVE dataset is one clean example within a large collection of partly corrupted displacement fields. Hence it is a step towards efficient information extraction, though the implemented voting has many potential ~~aspects of improvements~~areas for improvement.

4.3 Validation over stable terrain

A second component for validation is an analysis of the stable ground, and the effect of the smoothing of the voted estimates. The non-glaciated terrain ~~are the locations stemming~~ is taken from a mask. A similar mask, also based on the Randolph glacier inventory, is used within the GoLIVE pipeline. Here, displacements over land and non-glaciated terrain are used to co-align the imagery ~~Fahnestock et al. (2016)~~(Fahnestock et al., 2016), as geo-location errors might be present in the individual Landsat ~~imagery~~images. The fitting is done through a polynomial fit~~, still, ~~; in general these offsets should be random ~~, and its mean should be zero~~ with a zero mean.

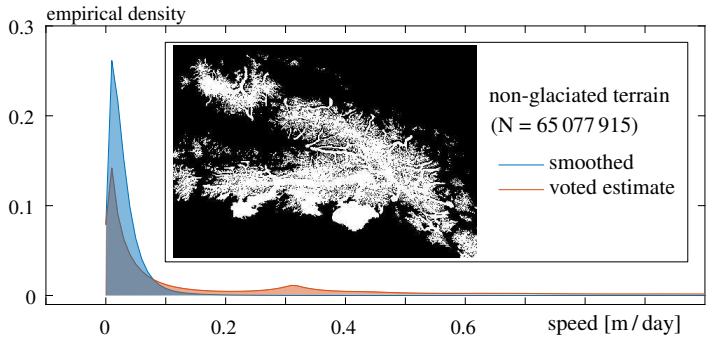

Figure 10. Distribution of the speed over stable terrain, for displacements extracted from the voting process, or after spatial temporal smoothing. The mask used is within the inset.

The distribution of these stable terrain measurements, more than 65 million in total, are illustrated in ~~figure~~Figure 10. Similar to the visual inspection already illustrated in Figure 6b, the distributions also show a clear improvement~~. This is a welcome~~

property as , even though the voted estimates still seem to be noisy with significant outliers.

4.4 Glaciological observations

When looking at the spatio-temporal dataset some patterns that are have been observed by others also appear in our dataset. For example, the full extent of Bering glacier slows down, as highlighted by Burgess et al. (2012), however our time series cover covers a period where the full deceleration towards a quiescent state can be seen. This observation of a slow down can also be made for Donjek Glacier (Abe et al., 2016) and Logan Glacier (Abe and Furuya, 2015), see suplementary supplementary video. In the time period covered by our study some surges appear to initiate. For example, our dataset comprises captures a surge traveling along the main trunk of Klutlan Glacier , see also Figure(see Figures B1&B2 in the appendix).

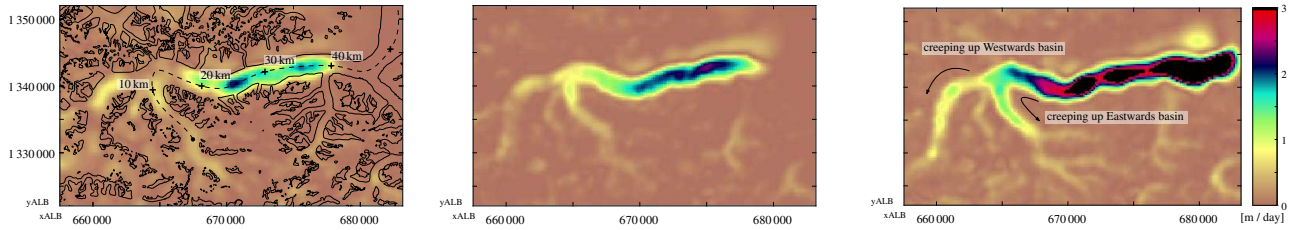

(a) 20 Jul 2014 - 21 Aug 2014 (b) 1 Mar 2015 - 2 Apr 2015 (c) 23 Jun 2016 - 25 Jul 2016

Figure 11. Snapshots of ice speeds at different time instances from a data compilation for the summer 2016 surge occurring on Klutlan Glacier (for location see Figure 7). The used GoLIVE data configuration is shown in Figure A1, and the data is from the smoothed dataset.

When looking at the surge occurring at For the surge of Klutlan Glacier, the dataset does capture shows the evolution of its dynamics, as can be seen in Figure 12. The surge initiation seems to happen in the central trunk of the glacier, as and the surge front progresses downwards from there (with steady bulk velocities around four meters per day). The surge also propagates upwards mainly into the most westwards westernmost basin. The eastward basin does also eastern basin does increase in speed, but to a lesser extent, while the middle basin of this glacier system does not seem to be affected significantly. Though, its extent is mostly pronounced in the lower part of the glacier, as the upward creep of The up-glacier velocity increase is limited and does not reach the headwalls of any basin. In Landsat imagery of late 2017, there is no indication of any heavily crevassed terrain in the upper parts of these basins, which supports the hypothesis of a partially developed surge.

When looking at the velocities over the flowline of the Klutlan glacier, as in Figure 12a, both the extension downstream as well as the upstream progression of the surge can be seen. Most clearly, the surge front seems to propagate downwards with a steady velocity, but seems to slow down around the 50 km mark (see dashed line in Figure 12a), as shown by the break in slope. Here, the glacier widens but the surge does continueinto a lobe at the terminus. This can suggest ice thickness is homogeneous

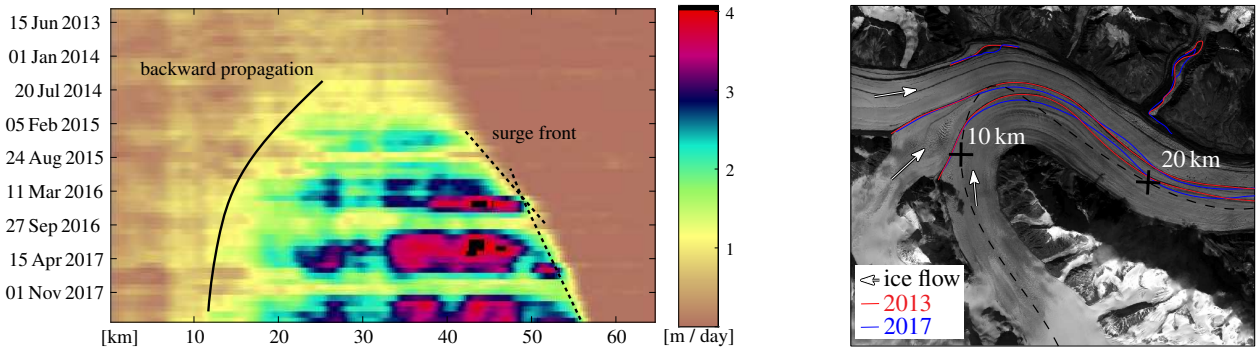

(a) Speed along flowline of Klutlan Glacier, line given in Figure 11a.

(b) Moraine positions

Figure 12. The speed over the central flowline of Klutlan Glacier. The markings of this flowline are shown in figure 11a. In Figure 12b the convergence of different basins of the Klutlan glacier is shown, data is from a RapidEye acquisition on the 5th of September 2013 and at the 23rd of September 2017. For comparison the 2013 image is overlain with the two ~~morraine~~ moraine positions.

here or ice thickness does not seem to play an important role in surge propagation.

At the end of the summer of 2016 the tributary just north of the 20 kilometer mark of ~~klutlan~~ Klutlan Glacier seems to increase in speed. This can be confirmed by tracing the extent of the looped moraines, as in Figure 12b. In the same imagery the medial moraines of the meeting point of all basins are mapped as well. Here, the moraine bands before and after the event align well ~~in~~ at the junction, indicating a steady or similar contribution over the full period. Or an insignificant effect, as the surge has not been developing into very fast flow. In contrast, the lower part of this glacial trunk has moraine bands that do not align.

The surge behavior we observe for Klutlan Glacier~~is not a special mechanism and similar propagationbehaviour~~ , especially the propagation, can be observed at other glaciers within the ~~mountain ranges~~study area. For Fisher Glacier, a similar increase in speed is observed within the main trunk that later propagates downstream as well as upstream. ~~Similarly, this~~ This also seems to be the case for Walsh Glacier, where a speed increase ~~at~~ in the eastern trunk ~~triggers~~ leads to a surge on the northern trunk ~~leading to~~ and a glacier-wide acceleration. On its way the fast flowing ice initiates surges in tributaries downflow, but the surge extent also ~~creeps~~ moves upslope and tributaries that were ~~more~~ further up-glacier from the initial surge start to speed up. This is also ~~true~~ seen for Steele Glacier, ~~that develops into~~ which develops a surge and Hodgson Glacier is ~~entrained into this~~ later entrained into the fast flow as well.

These ~~analysis were~~ analyses are best observed with the help of an animation (see supplement) but the initial identification was done through a simple visualization of the spread of flow speed ~~,~~ (see Figure 13). Here the surging glaciers stand out, ~~but also~~ also do most of the tidewater glaciers, which have a highly dynamic nature at their fronts. ~~Not only large glaciers can be~~

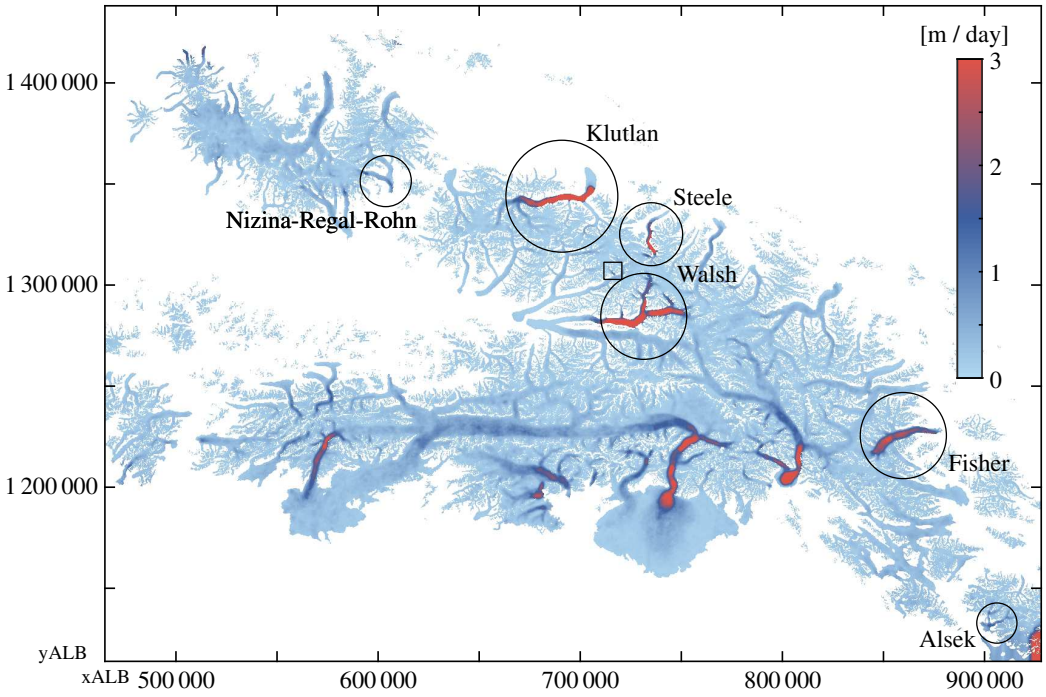

Figure 13. Spread of variation in flow speed (using the difference between the 20th and 80th percentile) over the observed period (2013-2018). Different dynamic glaciers are encircled, and the square indicates the tributary glacier shown in Figure C1.

~~identified but also the dynamics~~ Dynamics in smaller tributaries ~~. For~~ are visble as well, for example, a tributary of the Chitina Glacier seems to have pushed itself into the main trunk within a two-year time-period, see figure C1 in the appendix.

5 ~~Discussions~~Discussion

Synthesized velocity ~~estimates~~ time-series estimated from our post-processing chain of GoLIVE image-pair velocity determinations are dependent on the number and distribution of measured displacements (see Appendix A). ~~Surface features~~ It may be possible to improve these time-series in several ways. Surface features imaged in the same season have similar appearances, ~~thus~~ allowing good displacement fields ~~can be estimates from imagery~~ to be produced from images which are a year apart, as is typical working practice (Heid and Kääb, 2012b; Dehecq et al., 2015). ~~Such annual~~ Annual displacements fields could be helpful when areas are cloud covered for long periods, ~~such estimates can then~~ as these estimates can function as gap fillers in the least squares estimation. ~~Furthermore,~~ Because the adjustment model assigns equal weighting to individual displacements if no other information is available~~. Hence ~~, some velocity changes might be missed or blurred in time. Such a drawback might be overcome with spatial constraints, such as an advection pattern imposed on the data, although this would increase the

amount of post-processing.

Another limitation of our method concerns the glacier kinematics that are constrained by our model. In the current implementation the deviation (σ) is dependent on the time interval. From a measurement perspective this makes sense, but the model does ~~thus~~ not inherently account for speed change. ~~Hence, for~~ For long time intervals the fuzzy function forces the deviation to become ~~slim~~small. This reduces the ability to get a correct match ~~, especially~~ when glacier-dynamical changes are occurring. It might ~~therefore be worthwhile~~ be helpful to explore the ~~improvements occurring~~ improvement when a fixed deviation is set instead. In addition, ~~the low score~~ low scores over glaciated terrain ~~, might indicate~~ might indicate that the deviation of the displacement is set too tight. When this deviation is given higher bounds, the score increases~~and such parameter~~ , and such behavior can then be used as a meaningful measure.

The smoothing parameter used is a single global parameter that assumes isotropy. In order to fulfill this property the spatio-temporal data has been scaled accordingly. However, when severe data gaps are present, the velocity dataset still ~~seems to jump~~shows jumps. This will improve when more data is available, for example by including Sentinel-2 data or ~~incorporate~~ incorporating across-track matching (Altena and Kääb, 2017a). An increase in votes will result in a better population of the vote space, as can be seen in Figure 6. In addition, the voting score, that is the consensus score in the Hough space, can be used ~~for~~ as the initial weighting for the smoothing procedure (w in equation 2). This might reduce the ~~amount~~ number of iterations used by the robust smoother. ~~Nonetheless, much improvement~~ Improvement can be made ~~by~~ to the smoother, as ~~it~~ our initial implementation has a simple neighborhood function and has no knowledge of glacier specific properties.

6 Conclusions

In ~~the past couple of~~ five years the increase in the number of high quality optical satellite systems have made it possible to extract detailed and frequent velocity fields over glaciers, ice caps and ice sheets. The GoLIVE dataset is a repository of such velocity fields derived from Landsat 8, ~~and~~ available at low latency for analysis by the community. Discovery and exploration of this resource can be complicated due to its vast and growing volume, and the complexity of spatio-temporal changes of glacier flow fields. ~~Hence, in~~ In this study we introduce an efficient post-processing scheme to combine ice velocity data from different ~~, but~~ overlapping time-spans. The presented methodology is resistant to multiple outliers, as voting is used instead of testing. However, since cloud cover ~~can still~~ or surface change can hamper velocity estimation and spatial flow relations are not incorporated, the resulting synthesized time-series still have gaps or outliers. We use a data-driven spatio-temporal smoother to address this issue and enhance the visualization of real glacier flow changes.

Our synthesized time-series has a monthly (32 days) temporal interval and 300 meter spatial resolution. The time-series spans 2013 to 2018 and covers the Saint Elias Mountains and vicinity. Within this study area, we identify several surges ~~in~~ of

different glaciers at different times and their development over time can be observed. Such details can even be extracted for small tributary glaciers. Even velocities for the snow-covered upper glacier areas are in general estimated accurately. Thus our synthesized time-series can provide an overview of where and when interesting glacier dynamics are occurring.

This study is a demonstration of the capabilities of the new GoLIVE-type remote sensing products combined with an advanced data filtering and interpolation scheme. We demonstrate that our method can be implemented with ease for a large region, covering several mountain ranges. The derived smoothed time-series data contains many subtle additional changes that could be investigated. If this time-series is combined with digital elevation model (DEM) time-series (Wang and Kääb, 2015), it becomes possible to look at changes in ice ~~flux~~ mass in great detail.

The presented velocity time-series has a high temporal dimension, especially in respect to the sensor 16-day orbit repeat cycle. Though temporal or spatial data-gaps are still present (due to the short temporal interval, cloud cover or visual coherence loss) this might partly be addressed by enlarging the temporal resolution or through additional data, such as from Sentinel-2 (Altena and Kääb, 2017a). Fortunately, harmonization with other velocity datasets can be easily implemented, because our procedure uses only geometric information and ~~are~~ is not dependent on sensor type. With our framework it is thus possible to make a consistent time-series composed of a patchwork of optical or SAR remote sensing products.

Data availability. The Global Land Ice Velocity Extraction from Landsat 8 (GoLIVE) data is available at nsidc.org/data/golive (dx.doi.org/10.7265/N5ZP442B)

Appendix A: ~~Used velocity~~ Velocity pairs used

The GoLIVE velocity fields used in this study are of a considerable amount. In order to get an overview of the data used, the velocity pairs are plotted ~~in data graphs. In the example of Figure ?? the graph is annotated with dates, in order to better understand the other graphs corresponding to other path and rows which are given afterwards. Within the graph each gray arch represent a displacement field used in this study. The nodes of these arches come down to certain dates, where time is oriented counter clockwise. The colored lines represent year marks and are in correspondence with the colored footprints used in~~ as a network of edges through time, in Figure A1. Every red arch corresponds to a displacement estimate over a certain period, with a specific footprint (a given path row combination, see Figure 1 for localization). The general statistics of the collection of used GoLIVE displacement pairs are given in the table A1.~~For sake of simplicity, dates are removed from all other graphs.~~

~~time-~~

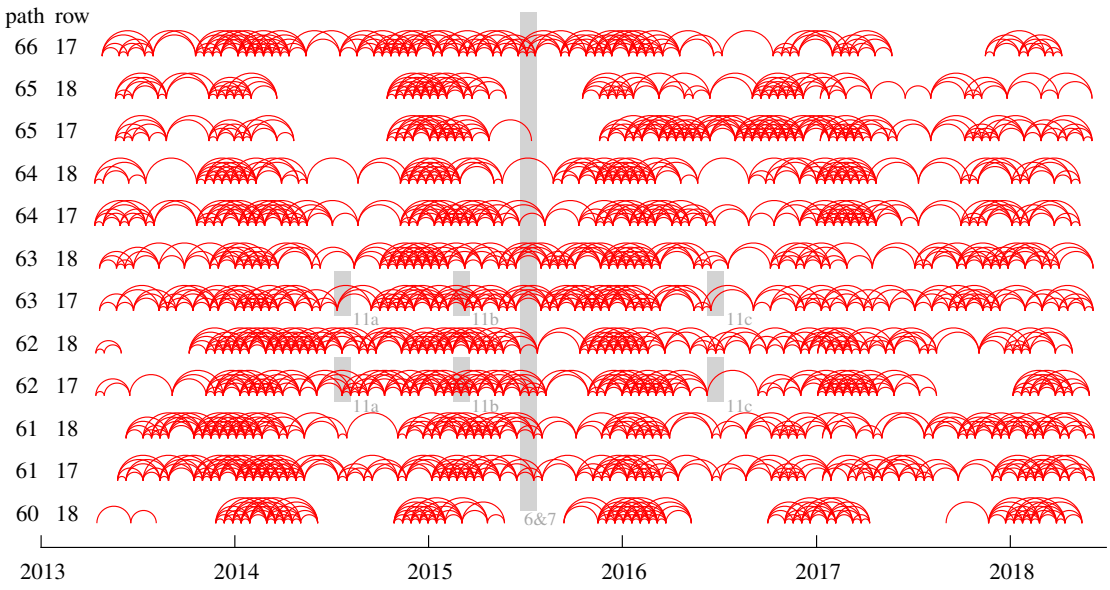

Figure A1. Node network of the velocity fields used in this study, a total of 2736 velocity fields. The gray bars span the time interval used for the generation for the different velocity products used in the figures in the main text. The specific numbering is given by their annotation, which is also in gray.

time-interval	60	61		62		63		64		65		66	path
~~interval~~ in days ↓	18	17	18	17	18	17	18	17	18	17	18	17	row
16	34	45	43	43	47	41	43	41	38	42	29	41	
32	34	40	37	46	49	46	39	38	34	40	27	39	
48	33	46	43	41	47	43	40	43	31	38	28	38	
64	27	47	42	41	42	44	40	36	26	38	25	38	
80	26	41	37	42	45	47	38	41	31	37	22	35	
96	21	38	38	38	43	42	40	40	35	30	21	35	

Table A1. number of GoLIVE displacement products used in the generation of the product, ordered by location through path, row and by relative time-interval.

Appendix B: Corrections done by smoothing

In the following section plots are given of speed variations over selected areas of interest, the locations are denoted in Figure ~~??~~ B1&B2 by red crosses. Every plot has a bloxplot with the least squares estimate of a selection of observations. This selection was done through consensus, by voting as described in the paper. The gray lines indicate the smoothed spatio-temporal velocity. These are multiple lines, as not one estimate is taken, but a surrounding area of 5x5 pixels wide neighborhood is taken. This is done in order to have sufficient data points and see the spread of the observations and the influence of the smoother. A comparison between both estimated and smoothed version is shown in the right graph of each figure, where the white line indicates the 1:1.

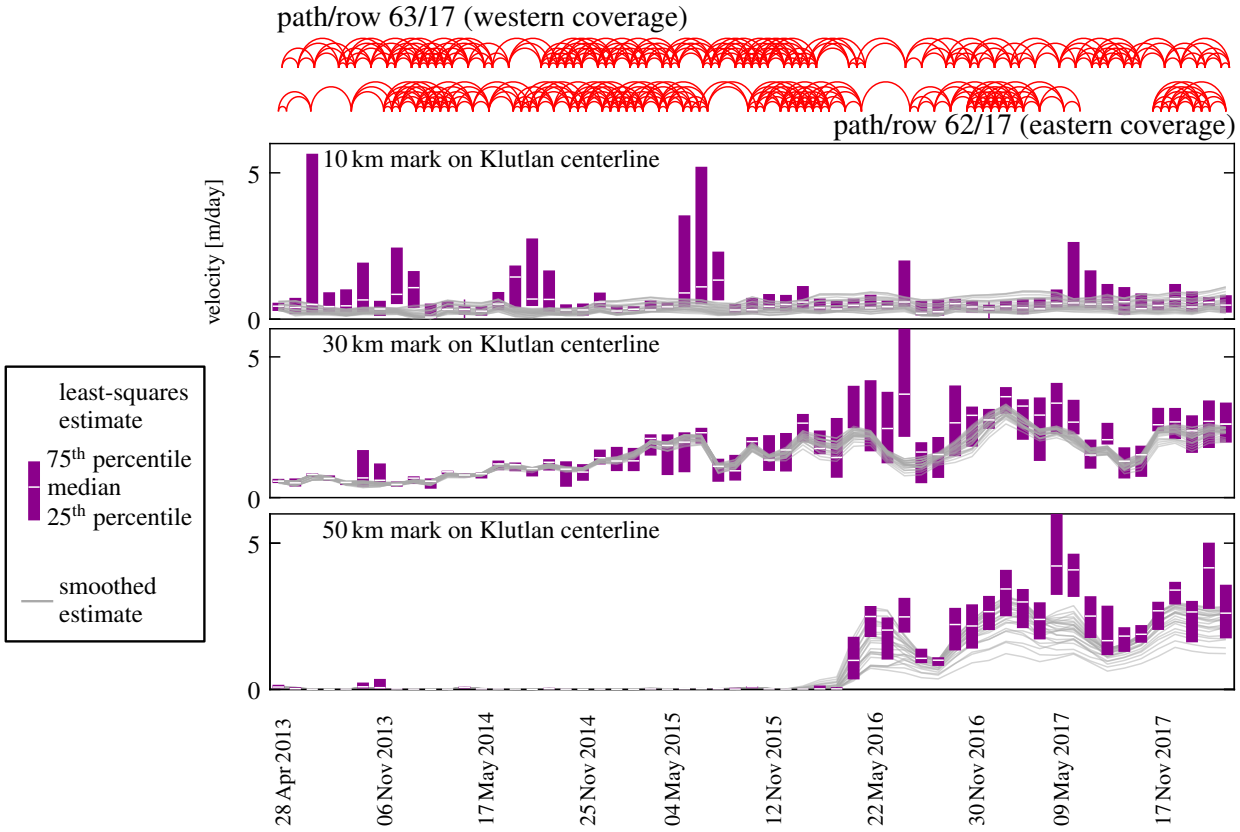

Figure B1. Temporal evolution of three locations along the flowline of Klutlan Glacier. The data from the specific marker and its direct neighborhood is shown. In purple is the boxplot of this data, while in gray, the smoothed estimates are plotted. For the location of the reference marks, please see Figure ~~12~~11a. Above the figures, the network configuration of the GoLIVE data for the two covering Landsat scenes is given.

Figure B3 shows the velocity evolution of the ocean terminating part of Hubbard Glacier (see figure 7 for specific localization). This glacier is seen from path 61&62 and is in row 18. Data is coming from the GoLIVE dataset and an open configuration

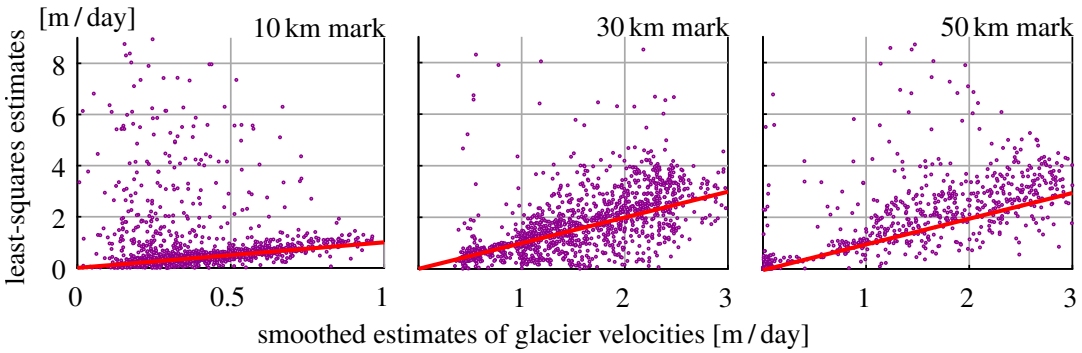

Figure B2. The temporal data shown in Figure B1 is combined and the least squares consensus is plotted against the smoothed estimate. The slanted line in all figures corresponds to the 1:1.

is used for the estimation of the velocity. Aliasing occurs both in the slow moving part (0-4 km) and the fast moving part (5-7 km). The availability of displacement data from GoLIVE is mostly in the winter, as can be seen in Figure A1. Late in 2015 the Hubbard Glacier seems to slow down completely. However, at the same period the amount of GoLIVE displacement data is relatively sparse. When a lack of data occurs, it is very difficult to establish consensus and extract information. To some degree this seems to occur for other autumn seasons as well.

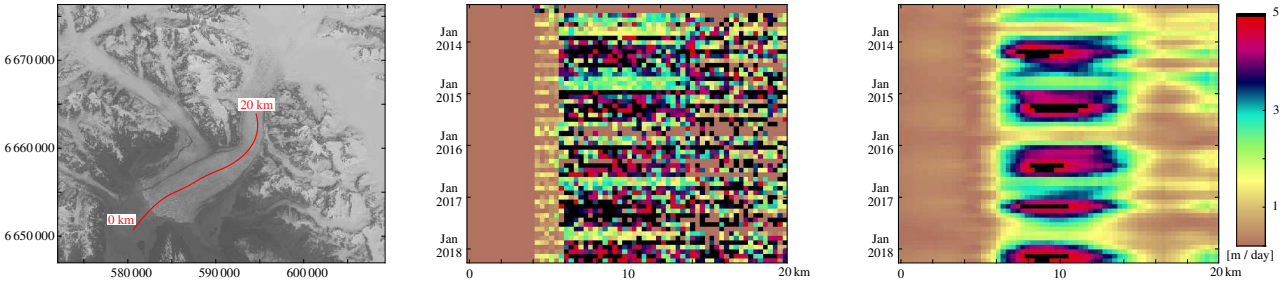

(a) Landsat 8 acquisition. (b) Raw least squares estimate. (c) Smoothed estimate.

Figure B3. B3a) Landsat 8 acquisition on the 5th of September 2013 over Hubbard Glacier, in red is the centerline used for the sampling which is plotted in figure B3b&B3c. B3b) velocity estimates using the data of displacements that had consensus during the voting step. B3c) smoothed estimate of velocity evolution over time, using spatial and temporal data and assisted by a off-glacier mask.

Appendix C: Tributary dynamics

From the constructed multi-temporal time-series the variance of a low and high quantile can be estimated. This gives an overview of ice masses with a highly dynamic nature. Through this simple analysis, an unknown tributary surge was identified.

The push of this tributary into the medial moraine and its velocity record over time can be seen in Figure C1.

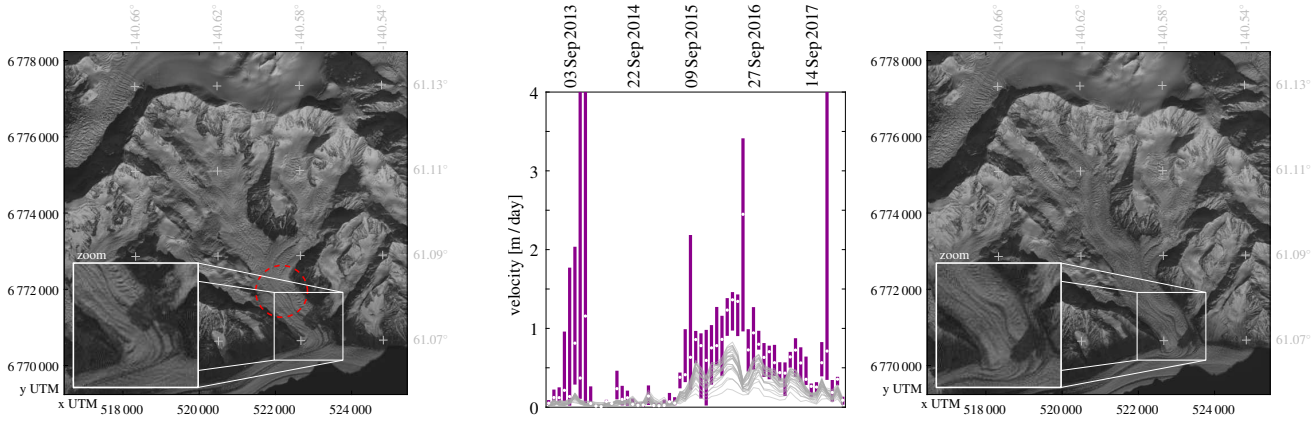

(a) 24 Sep 2014 (b) estimated velocities (c) 23 Sep 2017

Figure C1. A tributary of Chitina Glacier surged in the period 2015-2016. Images are both acquired by Landsat 8, its location is indicated by a square in figure 13. The location of the time-series in figure C1b, is indicated by a red dashed circle in figure C1a.

Author contributions. Bas Altena led the development of this study. All authors discussed the results and commented on the manuscript at all stages.

Competing interests. All authors declare no competing interests.

Acknowledgements. The research of B.A. and A.K. has been conducted through support from the European Union FP7 ERC project ICE-MASS (320816) and the ESA projects Glaciers_cci (4000109873 14 I-NB) and ICEFLOW (4000125560 18 I-NS). This work was supported by USGS award G12PC00066. The GoLIVE data processing and distribution system is supported by NASA Cryosphere award NNX16AJ88G. The authors are grateful to Planet Labs Inc for providing RapidEye satellite data for this study via Planet's Ambassadors Program.

References

Abe, T. and Furuya, M.: Winter speed-up of quiescent surge-type glaciers in Yukon, Canada, The Cryosphere, 9, 1183–1190, https://doi.org/10.5194/tc-9-1183-2015, 2015.

Abe, T., Furuya, M., and Sakakibara, D.: Brief Communication: Twelve-year cyclic surging episodes at Donjek Glacier in Yukon, Canada, The Cryosphere, 10, 1427–1432, https://doi.org/10.5194/tc-10-1427-2016, 2016.

Altena, B. and Kääb, A.: Elevation change and improved velocity retrieval using orthorectified optical satellite data from different orbits, Remote Sensing, 9, 300, https://doi.org/10.3390/rs9030300, 2017a.

Altena, B. and Kääb, A.: Weekly glacier flow estimation from dense satellite time series using adapted optical flow technology, Frontiers in Earth Science, 5, 53, https://doi.org/10.3389/feart.2017.00053, 2017b.

Arendt, A., Luthcke, S., Gardner, A., O'neel, S., Hill, D., Moholdt, G., and Abdalati, W.: Analysis of a GRACE global mascon solution for Gulf of Alaska glaciers, Journal of Glaciology, 59, 913–924, https://doi.org/10.3189/2013JoG12J197, 2013.

Arendt, A. A.: Assessing the status of Alaska's glaciers, Science, 332, 1044–1045, 2011.

Armstrong, W. H., Anderson, R. S., and Fahnestock, M. A.: Spatial patterns of summer speedup on South central Alaska glaciers, Geophysical Research Letters, 44, 1–10, https://doi.org/10.1002/2017GL074370, 2017.

Baarda, W.: A testing procedure for use in geodetic networks, Rijkscommissie voor Geodesie, 1968.

Berthier, E., Schiefer, E., Clarke, G. K., Menounos, B., and Rémy, F.: Contribution of Alaskan glaciers to sea-level rise derived from satellite imagery, Nature Geoscience, 3, 92, https://doi.org/10.1038/ngeo737, 2010.

Bieniek, P. A., Bhatt, U. S., Thoman, R. L., Angeloff, H., Partain, J., Papineau, J., Fritsch, F., Holloway, E., Walsh, J. E., Daly, C., et al.: Climate divisions for Alaska based on objective methods, Journal of Applied Meteorology and Climatology, 51, 1276–1289, 2012.

Burgess, E., Forster, R., Larsen, C., and Braun, M.: Surge dynamics on Bering Glacier, Alaska, in 2008-2011, The Cryosphere, 6, 1251, https://doi.org/10.5194/tc-6-1251-2012, 2012.

Burgess, E. W., Forster, R. R., and Larsen, C. F.: Flow velocities of Alaskan glaciers, Nature communications, 4, 2146, https://doi.org/10.1038/ncomms3146, 2013.

Clarke, G. K. and Holdsworth, G.: Glaciers of the St. Elias mountains, US Geological Survey professional paper, 2002.

Copland, L., Pope, S., Bishop, M. P., Shroder, J. F., Clendon, P., Bush, A., Kamp, U., Seong, Y. B., and Owen, L. A.: Glacier velocities across the central Karakoram, Annals of Glaciology, 50, 41–49, 2009.

Dehecq, A., Gourmelen, N., and Trouvé, E.: Deriving large-scale glacier velocities from a complete satellite archive: Application to the Pamir–Karakoram–Himalaya, Remote Sensing of Environment, 162, 55–66, https://doi.org/10.1016/j.rse.2015.01.031, 2015.

Fahnestock, M., Scambos, T., Moon, T., Gardner, A., Haran, T., and Klinger, M.: Rapid large-area mapping of ice flow using Landsat 8, Remote Sensing of Environment, 185, 84–94, https://doi.org/10.1016/j.rse.2015.11.023, 2016.

Fatland, D. R. and Lingle, C. S.: InSAR observations of the 1993-95 Bering Glacier (Alaska, USA) surge and a surge hypothesis, Journal of Glaciology, 48, 439–451, https://doi.org/10.3189/172756502781831296, 2002.

Fischler, M. A. and Bolles, R. C.: Random sample consensus: a paradigm for model fitting with applications to image analysis and automated cartography, Communications of the ACM, 24, 381–395, https://doi.org/10.1145/358669.358692, 1981.

Garcia, D.: Robust smoothing of gridded data in one and higher dimensions with missing values, Computational statistics & data analysis, 54, 1167–1178, https://doi.org/10.1016/j.csda.2009.09.020, 2010.

Gardner, A. S., Moholdt, G., Cogley, J. G., Wouters, B., Arendt, A. A., Wahr, J., Berthier, E., Hock, R., Pfeffer, W. T., Kaser, G., et al.: A reconciled estimate of glacier contributions to sea level rise: 2003 to 2009, science, 340, 852–857, https://doi.org/10.1126/science.1234532, 2013.

Han, J., Kóczy, L., and Poston, T.: Fuzzy Hough transform, Pattern recognition letters, 15, 649–658, https://doi.org/10.1016/0167-8655(94)90068-X, 1994.

Harig, C. and Simons, F. J.: Ice mass loss in Greenland, the Gulf of Alaska, and the Canadian Archipelago: Seasonal cycles and decadal trends, Geophysical Research Letters, 43, 3150–3159, https://doi.org/10.1002/2016GL067759, 2016.

Heid, T. and Kääb, A.: Evaluation of existing image matching methods for deriving glacier surface displacements globally from optical satellite imagery, Remote Sensing of Environment, 118, 339–355, https://doi.org/10.1016/j.rse.2011.11.024, 2012a.

Heid, T. and Kääb, A.: Repeat optical satellite images reveal widespread and long term decrease in land-terminating glacier speeds, The Cryosphere, 6, 467–478, 2012b.

Herreid, S. and Truffer, M.: Automated detection of unstable glacier flow and a spectrum of speedup behavior in the Alaska Range, Journal of Geophysical Research: Earth Surface, 121, 64–81, https://doi.org/10.1002/2015JF003502, 2016.

Jeong, S., Howat, I. M., and Ahn, Y.: Improved multiple matching method for observing glacier motion with repeat image feature tracking, IEEE Transactions on Geoscience and Remote Sensing, 55, 2431–2441, https://doi.org/10.1109/TGRS.2016.2643699, 2017.

Kääb, A. and Vollmer, M.: Surface geometry, thickness changes and flow fields on creeping mountain permafrost: automatic extraction by digital image analysis, Permafrost and Periglacial Processes, 11, 315–326, https://doi.org/10.1002/1099-1530(200012)11:4<315::AID-PPP365>3.0.CO;2-J, 2000.

Kolaas, J.: Getting started with HydrolabPIV v1.0, Research report in mechanics 2016:01, University of Oslo, urn.nb.no/URN:NBN:no-53997, 2016.

Maksymiuk, O., Mayer, C., and Stilla, U.: Velocity estimation of glaciers with physically-based spatial regularization. Experiments using satellite SAR intensity images, Remote Sensing of Environment, 172, 190–204, https://doi.org/10.1016/j.rse.2015.11.007, 2016.

Meier, M. F. and Post, A.: What are glacier surges?, Canadian Journal of Earth Sciences, 6, 807–817, 1969.

Melkonian, A. K., Willis, M. J., and Pritchard, M. E.: Satellite-derived volume loss rates and glacier speeds for the Juneau Icefield, Alaska, Journal of Glaciology, 60, 743–760, https://doi.org/10.3189/2014JoG13J181, 2014.

Molnia, B. F.: Glaciers of Alaska, Alaska Geographic Society, 2008.

Moon, T., Joughin, I., Smith, B., Broeke, M. R., Berg, W. J., Noël, B., and Usher, M.: Distinct patterns of seasonal Greenland glacier velocity, Geophysical research letters, 41, 7209–7216, https://doi.org/10.1002/2014GL061836, 2014.

Muskett, R. R., Lingle, C. S., Tangborn, W. V., and Rabus, B. T.: Multi-decadal elevation changes on Bagley ice valley and Malaspina glacier, Alaska, Geophysical Research Letters, 30, https://doi.org/10.1029/2003GL017707, 2003.

Paul, F., Bolch, T., Kääb, A., Nagler, T., Nuth, C., Scharrer, K., Shepherd, A., Strozzi, T., Ticconi, F., Bhambri, R., et al.: The glaciers climate change initiative: Methods for creating glacier area, elevation change and velocity products, Remote Sensing of Environment, 162, 408–426, 2015.

Paul, F., Strozzi, T., Schellenberger, T., and Kääb, A.: The 2015 Surge of Hispar glacier in the Karakoram, Remote Sensing, 9, 888, https://doi.org/10.3390/rs9090888, 2017.

Pfeffer, W. T., Arendt, A. A., Bliss, A., Bolch, T., Cogley, J. G., Gardner, A. S., Hagen, J.-O., Hock, R., Kaser, G., Kienholz, C., et al.: The Randolph Glacier Inventory: a globally complete inventory of glaciers, Journal of Glaciology, 60, 537–552, https://doi.org/10.3189/2014JoG13J176, 2014.

Post, A.: Distribution of surging glaciers in western North America, Journal of Glaciology, 8, 229–240, 1969.

Quincey, D., Braun, M., Glasser, N., Bishop, M., Hewitt, K., and Luckman, A.: Karakoram glacier surge dynamics, Geophysical Research Letters, 38, https://doi.org/10.1029/2011GL049004, 2011.

Rosenau, R., Scheinert, M., and Dietrich, R.: A processing system to monitor Greenland outlet glacier velocity variations at decadal and seasonal time scales utilizing the Landsat imagery, Remote sensing of environment, 169, 1–19, https://doi.org/10.1016/j.rse.2015.07.012, 2015.

Rosenau, R., Scheinert, M., and Ebermann, B.: Velocity fields of Greenland outlet glaciers, Technische Universität Dresden, Germany, data1.geo.tu-dresden.de/flow_velocity/, 2016.

Rousseeuw, P. and Leroy, A.: Robust regression and outlier detection, vol. 589, John wiley & sons, https://doi.org/10.1002/0471725382, 2005.

Roy, D., Wulder, M., Loveland, T., Woodcock, C., Allen, R., Anderson, M., Helder, D., Irons, J., Johnson, D., Kennedy, R., Scambos, T., Schaaf, C., Schott, J., Sheng, Y., Vermote, E., Belward, A., Bindschadler, R., Cohen, W., Gao, F., Hipple, J., Hostert, P., Huntington, J., Justice, C., Kilic, A., Kovalskyy, V., Lee, Z., Lymburner, L., Masek, J., McCorkel, J., Shuai, Y., Trezza, R., Vogelmann, J., Wynne, R., and Zhu, Z.: Landsat-8: Science and product vision for terrestrial global change research, Remote Sensing of Environment, 145, 154–172, https://doi.org/10.1016/j.rse.2014.02.001, 2014.

Scambos, T., Dutkiewicz, M., Wilson, J., and Bindschadler, R.: Application of image cross-correlation to the measurement of glacier velocity using satellite image data, Remote Sensing of Environment, 42, 177–186, https://doi.org/10.1016/0034-4257(92)90101-O, 1992.

Scambos, T., Fahnestock, M., Moon, T., Gardner, A., and Klinger, M.: Global Land Ice Velocity Extraction from Landsat 8 (GoLIVE), Version 1, NSIDC: National Snow and Ice Data Center, Boulder, Colorado USA, https://doi.org/10.7265/N5ZP442B, nsidc.org/data/golive, 2016.

Scherler, D., Leprince, S., and Strecker, M. R.: Glacier-surface velocities in alpine terrain from optical satellite imagery - Accuracy improvement and quality assessment, Remote Sensing of Environment, 112, 3806–3819, https://doi.org/10.1016/j.rse.2008.05.018, 2008.

Skvarca, P.: Changes and surface features of the Larsen Ice Shelf, Antarctica, derived from Landsat and Kosmos mosaics, Annals of Glaciology, 20, 6–12, https://doi.org/10.3189/172756494794587140, 1994.

Strang, G. and Borre, K.: Linear algebra, geodesy and GPS, Wellesley-Cambridge Press, 1997.

Teunissen, P.: Testing theory, Delft Academic Press, 2000.

Turrin, J., Forster, R. R., Larsen, C., and Sauber, J.: The propagation of a surge front on Bering glacier, Alaska, 2001–2011, Annals of Glaciology, 54, 221–228, https://doi.org/10.3189/2013AoG63A341, 2013.

Van Wychen, W., Copland, L., Jiskoot, H., Gray, L., Sharp, M., and Burgess, D.: Surface velocities of glaciers in Western Canada from speckle-tracking of ALOS PALSAR and RADARSAT-2 data, Canadian Journal of Remote Sensing, 44, 57–66, https://doi.org/10.1080/07038992.2018.1433529, 2018.

Wackernagel, H.: Multivariate geostatistics: An introduction with applications, Springer Science & Business Media, https://doi.org/10.1007/978-3-662-05294-5, 2013.

Waechter, A., Copland, L., and Herdes, E.: Modern glacier velocities across the Icefield Ranges, St Elias Mountains, and variability at selected glaciers from 1959 to 2012, Journal of Glaciology, 61, 624–634, https://doi.org/10.3189/2015JoG14J14, 2015.

Wang, D. and Kääb, A.: Modeling glacier elevation change from DEM time series, Remote Sensing, 7, 10 117–10 142, https://doi.org/10.3390/rs70810117, 2015.

Westerweel, J. and Scarano, F.: Universal outlier detection for PIV data, Experiments in fluids, 39, 1096–1100, 2005.